Spatial Resolution and Processing Tradeoffs for HYDROS: Application of Reconstruction and Resolution Enhancement Techniques

David G. Long, *Senior Member, IEEE*, Michael W. Spencer, and Eni G. Njoku, *Fellow, IEEE*

***Abstract*—Recent developments in reconstruction and resolution enhancement for microwave instruments suggest a possible tradeoff between computation, resolution, and downlink data rate based on postcollection reconstruction/resolution enhancement processing. The Hydrospheric State mission is designed to measure global soil moisture and freeze/thaw state in support of weather and climate prediction, water, energy, and carbon cycle studies, and natural hazards monitoring. It will use an active and passive L-band microwave system that optimizes measurement accuracy, spatial resolution, and coverage. The active channels use synthetic aperture radar-type processing to achieve fine spatial resolution, requiring a relatively high downlink data rate and ground processor complexity. To support real-time applications and processing, an optional postcollection reconstruction and resolution enhancement method is investigated. With this option, much lower rate real-aperture radar data are used along with ground-based postprocessing algorithms to enhance the resolution of the observations to achieve the desired 10-km resolution. Several approaches are investigated in this paper. It is determined that a reconstruction/resolution enhancement technique combining both forward- and aft-looking measurements enables estimation of 10-km resolution or better backscatter values at acceptable accuracy. Key tradeoffs to achieve this goal are considered.**

***Index Terms*—Hydrospheric State (HYDROS), reconstruction, resolution enhancement.**

I. Introduction

A VARIETY of active microwave radar scatterometers have flown in space. These include the Earth Resources Satellite 1 and 2 (ERS-1 and ERS-2) and the Active Microwave Instrument (AMI) (1982–2001) [1], the NASA Scatterometer (1996–1997) (NSCAT) [2], and the SeaWinds scatterometer operated aboard QuikSCAT (1999–current) and ADEOS-2 (1999) [3]. Together, these instruments have demonstrated the utility of radar sensors in the study and monitoring of the earth's land, ocean, and atmosphere. The global coverage, but low resolution, of these sensors complements the high resolution, but limited coverage, of synthetic aperture radar (SAR) systems.

Previous scatterometers have been real-aperture radars that operate by transmitting a pulse of microwave energy toward the earth's surface and measuring the reflected energy. The backscattered energy is related to the normalized radar backscatter cross section (NRCS) via the radar equation [4]. The antenna beamwidth of the sensor determines the limiting spatial resolution of the NRCS observation, with typical resolutions varying from 25–50 km. Range processing may be employed, however, in order to improve the spatial resolution along the elevation axis of the footprint [20]. Scatterom have been primarily employed for the retrieval of near-surface winds over the ocean via measurements of the Bragg scattering from the wind-generated wave field of the surface [2], though scatterometer data are being applied to the study of tropical vegetation, polar ice, and global change (e.g., [5]–[10]). Scatterometer data are widely used in operational weather forecasting and sea ice monitoring.

In contrast, microwave radiometers are passive, receive-only sensors that measure the thermal emission (brightness temperature) of the target in the microwave band [4]. The apparent scene brightness temperature is related to the emissivity and temperature of the surface and is modified by moisture content and temperature of the intervening atmosphere. By appropriate selection of operating frequencies in several microwave bands, geophysical parameters such as the temperature and moisture content of the atmosphere, sea ice, and snow cover, as well as key surface properties such as land surface temperature [11], and soil and plant moisture (see [12]–[15] among others) can be estimated. The latter application concerns us here.

Improved soil moisture observations can be made with low-frequency radiometers by compensating for the effects of surface vegetation. Such compensation can be accomplished by using collocated scatterometer observations [16], [17]. The Hydrospheric State (HYDROS) mission was designed to obtain combined radiometer/scatterometer soil moisture retrievals [14], [18], [19]. To improve the spatial resolution of HYDROS soil moisture measurements, unfocused SAR processing is employed for processing HYDROS scatterometer measurements. SAR-type processing is computationally intensive and requires a large downlink data rate. To support weather prediction and near-real-time operational needs, the HYDROS mission will include an additional low bit-rate (LBR) downlink data stream containing lower resolution real-aperture measurements. Specialized ground-based processing will be applied to this low-resolution product to enhance the spatial resolution and reduce the data latency to operational users.

Recent developments in reconstruction and resolution enhancement for scatterometers [20] suggest a possible tradeoff between computation, resolution, and downlink data rate based

Manuscript received April 16, 2004; revised September 15, 2004. This work was supported by the National Aeronautics and Space Administration.

D. G. Long is with the Department of Electrical and Computer Engineering, Brigham Young University, Provo, UT 84602 USA (e-mail: long@ee.byu.edu).

M. W. Spencer and E. G. Njoku are with the Jet Propulsion Laboratory, California Institute of Technology, Pasadena, CA 91109 USA (e-mail: eni.g.njoku@jpl.nasa.gov).

Digital Object Identifier 10.1109/TGRS.2004.838385

on postcollection reconstruction/resolution enhancement processing. The fundamental processing theory of reconstruction and resolution enhancement is described in [5]. In this paper, we consider the application of this technique to the HYDROS mission. While focused on HYDROS, the results and analysis are applicable to other microwave sensors. Two approaches are considered: azimuth-only reconstruction and reconstruction by combining fore- and aft-facing looks. The latter approach, which has been successfully used with SeaWinds, proves most capable of achieving the highest resolution from low-resolution real-aperture HYDROS measurements; however, it requires modification of the instrument by collecting data throughout the antenna rotation. This paper is organized as follows: first, the HYDROS sensors are briefly described. Then, the study approach is described, and azimuth-only reconstruction is considered. Next, the combined fore/aft approach is evaluated and implementation tradeoffs considered. Finally, a brief conclusion is provided.

II. HYDROS Design Summary

A unique feature of HYDROS is its ability to obtain simultaneous active and passive (radar and radiometer) measurements of the surface, with resulting improvements in spatial resolution and accuracy of the derived products. The key derived products are soil moisture at 10-km resolution and freeze/thaw state at 3-km resolution. To generate these products, the HYDROS radar and radiometer sensors measure L-band (1.2–1.4 GHz) microwave emission and backscatter from the surface across a wide swath. The measurements are registered to an earth-fixed grid, providing updated global maps every three days at the equator and midlatitudes and more frequently at higher latitudes. The antenna is an approximately 6-m diameter deployable mesh reflector that provides 3-dB footprint sizes of approximately 40 km for the radiometer (dictated by the one-way gain pattern) and 28 km for the radar (dictated by the two-way gain pattern). The "single-look" radar resolution is enhanced to as fine as 300–700 m by using unfocused SAR processing that uses both range and Doppler processing [18]. From this, a multilook, calibrated output product is generated at 3-km resolution. The soil moisture product at nominal 10-km resolution is obtained by combining the 3-km radar data and 40-km radiometer data using optimal estimation. The radar measurements are more sensitive to the characteristics of vegetation cover, but provide a higher resolution downscaling capability when blended with the more accurate but coarser resolution radiometer measurements.

Key elements of the HYDROS system design are summarized in Table I. The HYDROS spacecraft is designed for a 670-km nearly circular sun-synchronous orbit, with equator crossings at 6 A.M. and 6 P.M. local solar time. The instrument combines radar and radiometer subsystems that share a single feedhorn and parabolic mesh reflector. The radar operates with (vertical) VV, (horizontal) HH, and (horizontal–vertical) HV transmit–receive polarizations, and uses separate transmit frequencies for the H (1.26 GHz) and V (1.29 GHz) polarizations to allow simultaneous operation. The partially polarimetric radiometer operates with V, H, and U (third Stokes parameter) polarizations at 1.41 GHz.

TABLE I
HYDROS Design Summary

Conically scanning, deployable mesh reflector
Simultaneous active and passive measurements at constant 40° incidence angle (shared antenna)
Radar:
1.26-1.29 GHz (VV, HH, HV)
3 km high-resolution (SAR processing)
6 x 28 km low-resolution (non-enhanced)
Radiometer:
1.41 GHz (V, H, U)
40 x 40 km resolution
Swath: 1000 km for frequent global mapping
Revisit:
3 days, global
1-2 days, above 45°N
Orbit:
670 km altitude
Sun-synchronous, 6 am / 6 pm

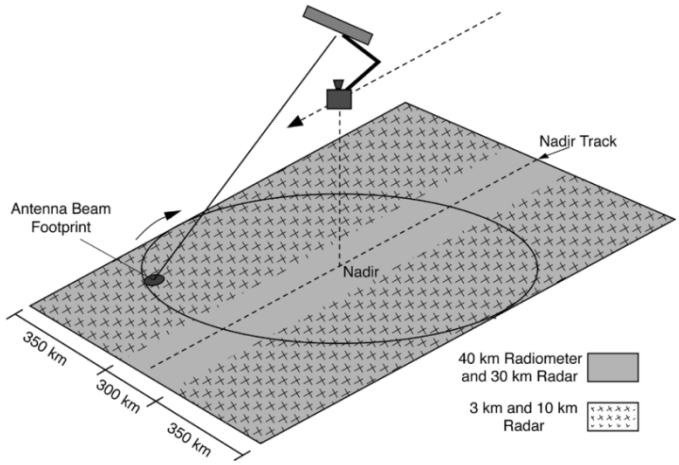

Fig. 1. HYDROS swath geometry illustrating the conical scanning geometry and various divisions of the swath. The total swath width is 1000 km.

The antenna reflector is offset from nadir and rotates about the nadir axis at 14.6 r/min, providing a conically scanning antenna beam with a surface incidence angle of approximately 40°. The fixed feedhorn does not rotate with the reflector. To maintain a polarization that is fixed with regard to the surface, the radar instrument assembly incorporates a pin polarizer that rotates synchronously with the reflector. Current plans are that the radiometer will not incorporate a polarizer due to insertion loss concerns, but the polarization rotation will be corrected in the ground processing. The antenna provides a radiometer footprint of approximately 40 km (root-ellipsoidal area) defined by the one-way 3-dB beamwidth. The two-way 3-dB beamwidth defines the real-aperture radar footprint of approximately 28 km. The coverage swath width of 1000 km provides global coverage within three days at the equator and two days at boreal latitudes ($>50^\circ$ N). Fig. 1 illustrates the instrument and conical scanning configuration.

To obtain the desired 3-km spatial resolution, the radar employs range and Doppler discrimination. While the unfocused SAR processing planned is similar to conventional SAR, the aperture length of HYDROS is quite short (32 ms), simplifying

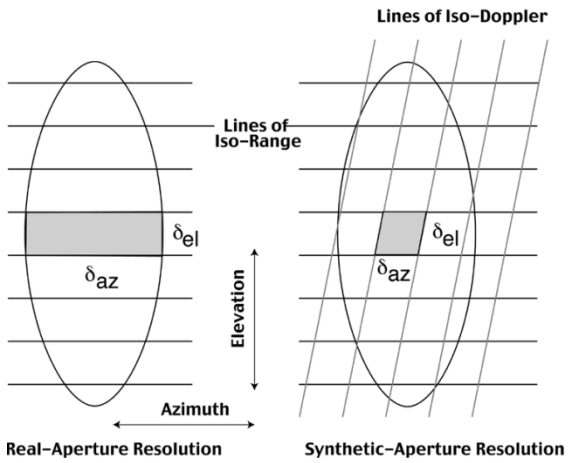

Fig. 2. HYDROS radar footprint geometry illustrating the iso-Doppler lines and iso-range lines at a particular swath location. Ovals represent the 3-dB antenna footprint. $\delta_{\rm az}$ and $\delta_{\rm el}$ represent the resolution in the azimuth and elevation direction, respectively. Note the varying relative orientations of the iso-Doppler and iso-range lines vary as a function of antenna rotation angle and, thus, with swath location.

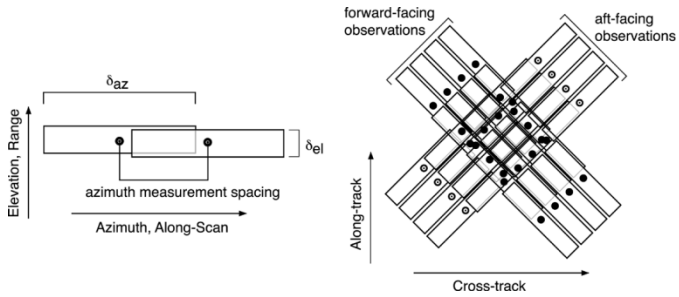

Fig. 3. (Left) Illustration of azimuth-only sampling. Slices at similar range from different pulses are combined in the azimuth direction. $\delta_{\rm az}$ and $\delta_{\rm el}$ represent the resolution in the azimuth and elevation direction, respectively. Dots indicate measurement centers. The goal of the reconstruction is to extract backscatter at this range at finer resolution in the azimuth direction. The effective resolution is limited by the spatial response function. (Right) Illustration of combined fore/aft measurements sampling. Multiple slices from multiple pulses from both forward and aft measurements are combined. Given backscatter measurements collected for each footprint, the 2-D backscatter is reconstructed over a fine grid [5].

the processing. Due to squint angle effects [20], the 3-km resolution cannot be achieved within a 300-km swath region centered on the nadir track (see Fig. 2). The 3-km resolution ("hi-res") portion of the swath is thus defined as the two outer 350-km-wide segments shown in Fig. 1.

The radiometer operates continuously, generating a relatively low (12.8-kp/s) data rate. In the baseline design, the radar delivers data in two modes: a high-resolution mode for generating 3- and 10-km geophysical products from SAR processing, and a low-resolution or real-aperture mode. In the high-resolution mode, each fully sampled radar return is digitized, compressed using block floating-point quantization (BFPQ), recorded by the onboard recorders, and later downlinked for range and azimuth compression processing on the ground. The peak instrument data rate is 31.7 Mb/s. In low-resolution mode, each radar return is incoherently averaged into ten range bins with phase information discarded. This averaging is done on the spacecraft, resulting in 6 km $\times$ 30 km cells and a 60.0-kp/s peak data rate, though 3-km averaging (at 120 kp/s) is also being considered and is thus used here. Individual averaged measurements are termed "slices" and are spaced approximately 3 km apart in azimuth and elevation. Radar low-resolution-mode data are continuously downlinked to support real-time and operational applications.

III. Study Methodology

The primary purpose of this paper is to evaluate the feasibility of using postprocessing reconstruction/resolution enhancement techniques applied to the HYDROS low-resolution radar data to support near-real-time processing without the need for SAR-like processing and its attendant high data rate. The goal is to achieve an effective resolution of 10 km with minimal data rate and ground computation.

In conducting this study, we are trying to minimize adverse impacts to the *existing* radar design, while enhancing the utility of the secondary low-rate data stream designed for real-time processing. In keeping with this philosophy, we only consider the real-aperture measurements that are preaveraged prior to transmission to the earth. (Phase information is not retained.) The high HYDROS pulse repetition frequency (PRF) of 3.5 kHz results in issuance of one pulse every 210 m along the beam rotational circumference (i.e., in the azimuth or along-scan direction). In the real-time downlink, the pulses are averaged down to an effective azimuth sampling of 3 km. For future reference, we note that the along-scan (azimuth) resolution without enhancement is approximately 28–30 km, corresponding to the two-way 3-dB antenna beamwidth in the azimuth direction. As previously noted, the onboard range processing performed prior to averaging results in a nominal effective range resolution of 6 km. Ground-based processing is used to reconstruct measurements to a higher effective azimuth resolution.

Advanced reconstruction and resolution enhancement techniques have proven to be very useful in improving the utility of scatterometer and radiometer data (e.g., see [8]). These techniques can be used to provide improved resolution measurements from microwave sensors and have been applied to scatterometers such as the NSCAT, the Seasat Scatterometer, the ERS-1/2 scatterometer, and the two SeaWinds scatterometers, as well as radiometers such as Scanning Multifrequency Microwave Radiometer and Special Sensor Microwave/Imager. The fundamental idea is to take advantage of the high-wavenumber information contained in oversampled measurements by reconstructing the aperture-filtered signal and inverting the spatial measurement response to estimate the radar backscatter (or brightness temperature in the case of radiom) at higher spatial resolution. Since enhancing the resolution also enhances the noise, there is a tradeoff between resolution enhancement and noise [5], [21], [22]. We note that the SeaWinds scatterometer has a similar antenna beamwidth, footprint, and geometry to the proposed HYDROS design. Resolution enhancement is being performed operationally on SeaWinds data for storm tracking, sea ice monitoring, and iceberg tracking.

It is proposed that the low-resolution mode HYDROS measurements be processed using a reconstruction algorithm to enhance the effective resolution. The reconstruction processing

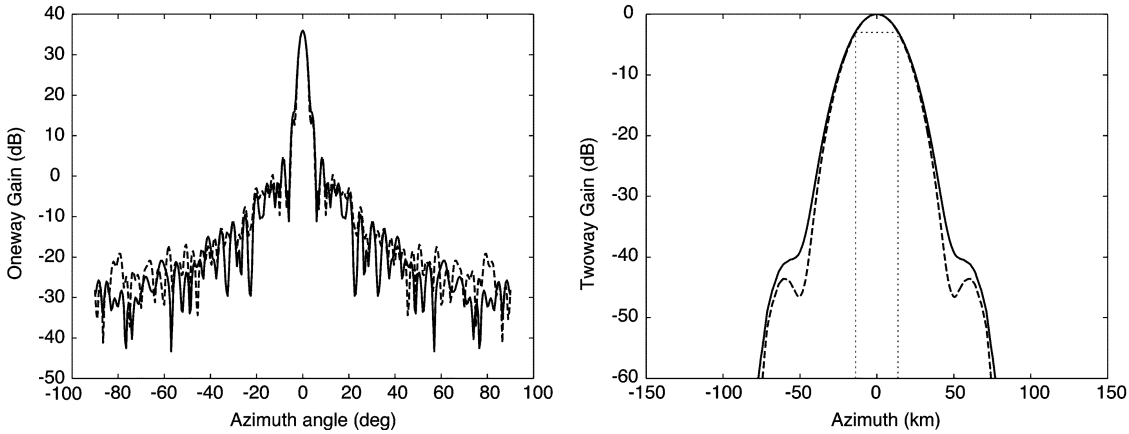

Fig. 4. (Left) HYDROS (solid) H and (dashed) V polarization azimuth antenna pattern: one-way gain versus azimuth angle. (Right) HYDROS (solid) H and (dashed) V polarization two-way azimuth response (which includes the effects of rotation between signal transmit and receive): gain versus along-rotation distance computed using nominal orbit geometry and rotation rate. Dotted gray box illustrates the 3-dB beamwidth.

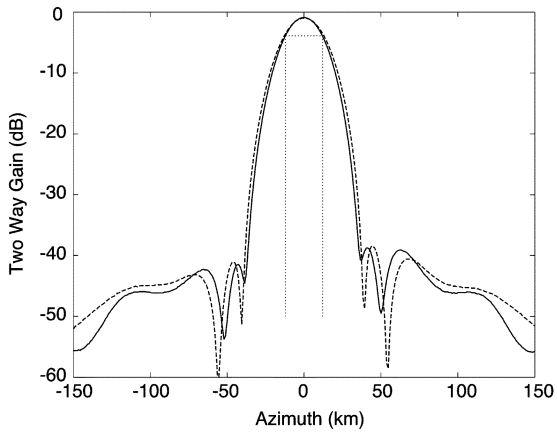

Fig. 5. QuikSCAT (outerbeam, solid) H and (inner beam dashed) V polarization azimuth response: gain versus along-rotation distance computed from left using nominal orbit geometry and rotation rate. Dotted gray box illustrates the 3-dB beamwidth. Compare with Fig. 4.

will estimate the surface backscatter at fine resolution from a dense array of aperture-filtered measurements. This is possible when the sampling is sufficiently dense and the spatial response function does not have spatial frequency nulls. The signal-to-noise ratio (SNR) must also be sufficient, since the inverse filtering which is part of the reconstruction tends to degrade the SNR [5].

As previously noted, two different approaches to HYDROS reconstruction and enhancement can be used. These are illustrated graphically in Fig. 3. Azimuth-only reconstruction is essentially a one-dimensional problem, while combined fore/aft reconstruction is a two-dimensional (2-D) problem. Note that unlike the coherent SAR-type processing, the reconstruction techniques used here are incoherent and thus have more limited resolution than the coherent processing, but also only need a lower downlink data rate.

For a single pulse, intrinsic resolution of the measurements in the azimuth (or rotation) direction is dictated by the 3-dB azimuth beamwidth of the antenna pattern, for HYDROS corresponding to approximately 28-km resolution (see Fig. 4). The antenna patterns shown are theoretical predicted patterns computed from a model of the HYDROS antenna courtesy of the Canadian Space Agency who are partners in the HYDROS mission. For comparison, Fig. 5 shows the measured QuikSCAT antenna azimuth response, which has a similar 3-dB width. (For reference, QuikSCAT rotates at 18 r/min, orbits at 800 km, and has a 1900-km wide swath, while HYDROS rotates at 14.6 r/min, orbits at 670 km, and has a 1000-km wide swath.)

IV. HYDROS Reconstruction/Enhancement

In conventional signal processing, reconstruction is achieved by low-pass filtering zero-hold data. Assuming the Nyquist rate is met, the effective resolution of such processing is typically limited to the size of 3-dB response of the spatial response function, in this case 28 km. However, higher resolution can be obtained using full reconstruction theory, which, in effect, convolves the measurements by the inverse spatial response function, i.e., deconvolving the spatial response function. We note that uniform sampling is not required for reconstruction, though it can simplify the processing. To be effective, the full reconstruction requires: 1) oversampling of the signal; 2) a spatial response that has no nulls in its spectrum over the desired frequency range; and 3) sufficiently high SNR, since the deconvolution tends to amplify high-frequency noise. If these requirements are met, the signal can be reconstructed to higher resolution than the 3-dB extent of the spatial response function. However, there is a tradeoff between reconstruction resolution and SNR degradation [5].

The results presented here are based on the iterative scatterometer image reconstruction (SIR) algorithm, modified for single-variate reconstruction [5], though other reconstruction techniques can be used. SIR has the advantage of not requiring uniform sampling and, compared to the Backus–Gilbert algorithm, requires less computation [21]. In any case, knowledge of the spatial response function and the sample locations is required [5], [22].

The primary limitation to reconstruction is the azimuth antenna pattern. The response pattern acts as a spatial filter on the surface. It must be inverted as part of the reconstruction. In effect, the reconstruction takes advantage of sidelobes in the response function to recover higher frequency information. If, however, the gain of the response pattern at any given spatial

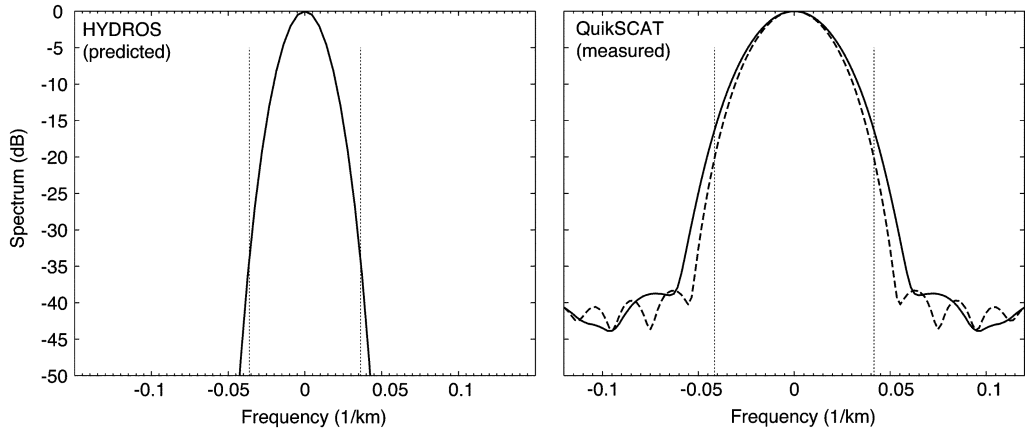

Fig. 6. (Left) Spectra of the predicted HYDROS azimuth response function (two-way antenna pattern including rotation effects). Dotted gray lines indicate the 3-dB beamwidth. (Right) Spectra of the measured QuikSCAT azimuth response function (two-way antenna pattern including rotation effects) for the (solid) outer and (dashed) inner beams.

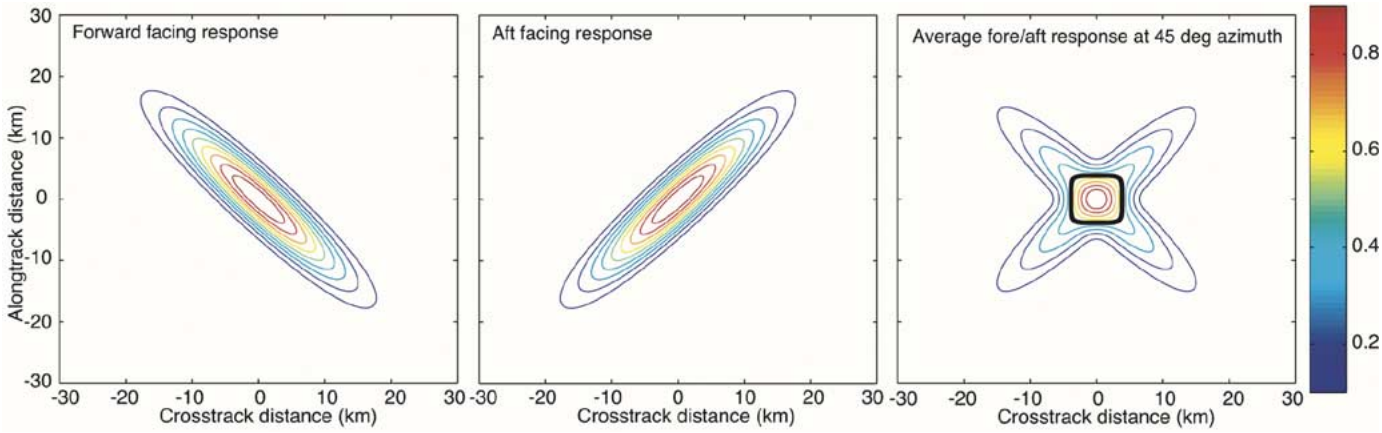

Fig. 7. Illustration of how combining forward-facing and aft-facing measurements can result in improved effective resolution. (Left) Contour plot of the spatial response function for a single range bin for a right side swath, forward-facing measurement. (Center) Contour plot of the spatial response function for a single range bin for a right side swath, aft-facing measurement at the same crosstrack swath location. (Right) Averaged fore/aft spatial response. Black contour corresponds to the 3-dB response, which is considerably smaller in the combined response than in the individual responses. Optimally combining multiple measurements distributed in two dimensions results in further improvement in the effective resolution over the 2-D image area.

frequency is too low, the signal cannot be recovered, since any noise present in the measurements at that frequency is overly amplified in the inversion. In this case, the noise dominates the signal. A practical limitation to the recovery is a response function spectral gain more than 40–50 dB down from the peak, though this number is reduced when the SNR is low.

Typically, radars (such as QuikSCAT) have higher antenna sidelobes with fairly broad spatial response patterns. However, radiometers typically require much lower sidelobes to improve their measurement accuracy. The HYDROS antenna design is driven primarily by the requirements for high-accuracy radiometer measurements. As a result, it has very low sidelobes with a narrow, low-pass spectrum. Fig. 6 contrasts the azimuth spectra of the HYDROS and QuikSCAT two-way antennas patterns. From this figure, it is clear that the HYDROS antenna pattern very nicely cuts off any information at spatial frequencies finer than about 20 km, while QuikSCAT, with its much less ideal antenna pattern, can achieve finer reconstruction, since some high spatial frequency information is retained, even though heavily attenuated.

In azimuth-only reconstruction, the reconstruction is performed only in the azimuth or rotation direction to improve over the real-aperture resolution defined by the rolloff of the antenna pattern. Range resolution remains unchanged. Simulations show that while the 3-dB azimuth resolution of HYDROS is 28 km, reconstruction resolution as fine as 22 km can be achieved—only a limited improvement due to the low HYDROS antenna pattern sidelobes. Thus, azimuth-only reconstruction cannot provide sufficient enhancement to improve the resolution from 28 km to the 10-km resolution desired for the soil moisture product. Instead, we examine 2-D reconstruction, which has been successfully used for other spaceborne radars including QuikSCAT [5], [8], [9].

Combining the forward-facing and aft-facing looks takes advantage of the finer intrinsic resolution of the HYDROS measurements in the range direction by combining, in ground processing measurements made when the antenna is facing forward with measurements made when the antenna is facing backward (see Figs. 3(b) and 7). However, it requires making measurements in two different azimuth look directions, requiring sampling around the 360° antenna rotation locus. We must also assume that the surface response is not azimuth angle dependent at the scales of interest. Studies using QuikSCAT data have revealed that this is a reasonable assumption at scales

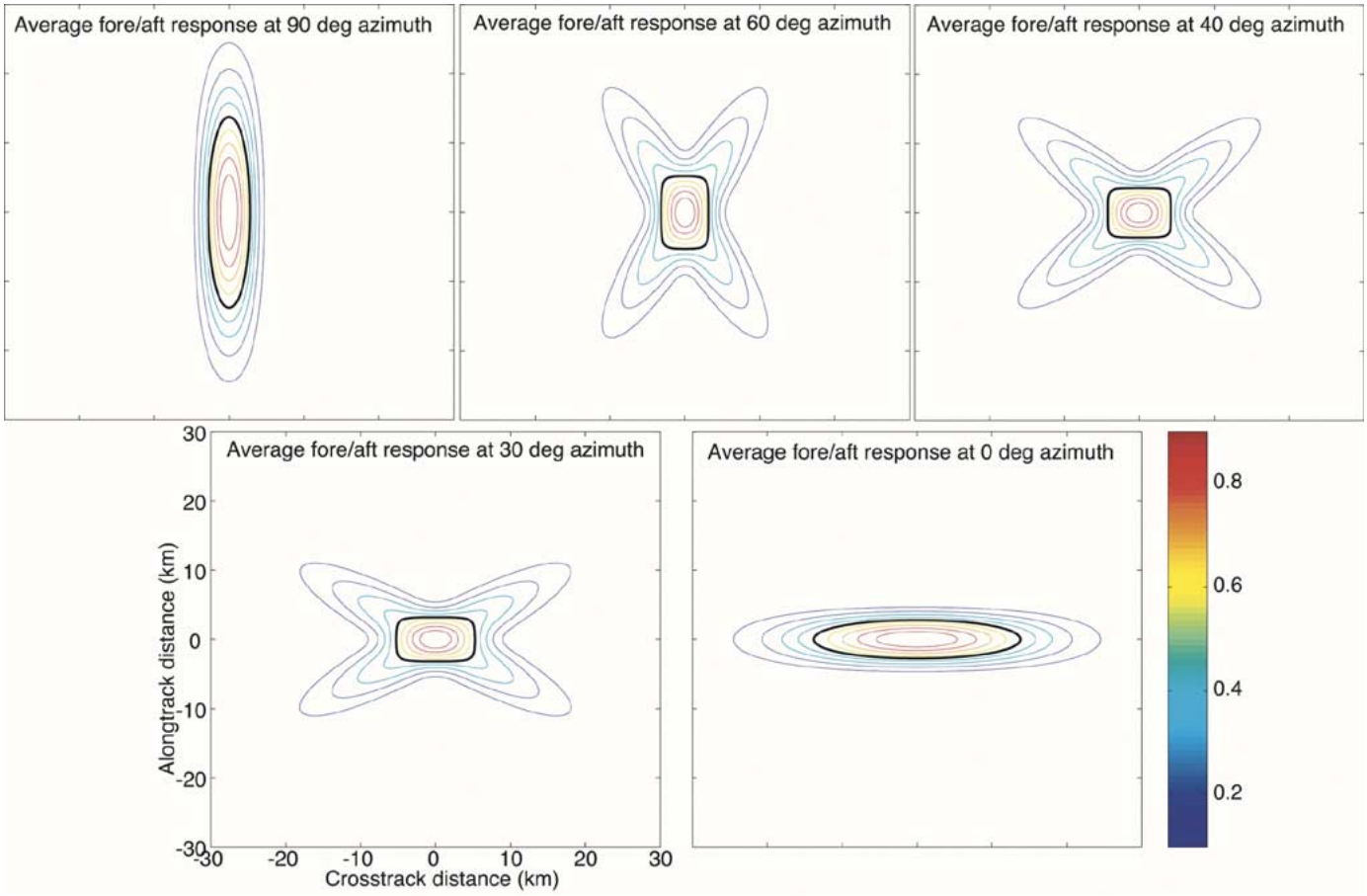

Fig. 8. Variation in fore/aft facing measurement orientation over the measurement swath results in variations in the effective resolution as indicated by the size/shape of the 3-dB contour (black contour) of the averaged fore/aft spatial response functions (shown left to right, top to bottom), which correspond to swath locations from the left side swath to the center swath. Compare with Fig. 7. Note that area and orientation of the 3-dB response varies across the swath.

of 3–5 km and larger over most land areas of the globe, making this approach feasible for resolution enhancement at this scale. We note that the baseline design includes only forward-looking measurements and, therefore, must be modified to make aft-facing measurements for this option. However, this change has a relatively small design impact on the HYDROS system.

As suggested by Fig. 7, the relative orientations of the slice spatial response patterns enable improved resolution, an idea suggested in [5]. Optimal resolution is obtained by reconstruction techniques using multiple overlapping measurements. We note that the recoverable resolution as determined by the spectra of the averaged slices is azimuth angle dependent (see Fig. 8), i.e., at a given swath location, depending on which direction is considered, the width of the main lobe of the spectra varies with direction. We, thus, consider both the best case and worst case spectral resolution. The best case resolution is the width of the 3-dB response in the orientation of the finest resolution, while the worst case resolution is the width of the 3-dB response in the orientation of the coarsest resolution.

Further, due to the measurement geometry, the relative orientation of the fore/aft measurements varies over the swath, causing variation in the reconstruction performance over the swath. Thus, reconstruction performance at different swath locations must be considered (see Fig. 8). As illustrated in Fig. 8, the best case (orientation of the direction of the finest resolution) and worst case (orientation of the direction of the coarsest resolution) combined fore/aft 3-dB resolution varies over the swath. While the reconstruction ameliorates this to a degree, spatial frequency components completely filtered out by the antenna pattern cannot be recovered.

We use simulation to evaluate the effective resolution of the reconstruction. Simulated measurements based on the predicted sampling and spatial response functions are generated with the aid of a synthetic truth image. Monte Carlo noise is then added [23], [24]. The noisy measurements are then processed using a reconstruction algorithm, and various metrics such as the effective resolution and the normalized standard deviation due to the noise are computed. In the following, reconstruction performance is evaluated using the iterative SIR algorithm with 500 iterations.

A metric for the noise level commonly used in scatterometer is the normalized standard deviation, referred to as "K_p." K_p of the raw measurements depends on the measurement SNR and the number of independent samples or 'looks' averaged in each measurement, i.e., [2]–[4]

$$K_p = \sqrt{\left\{\left[1+\left(\frac{2}{\mathrm{SNR}}\right)+\left(\frac{1}{\mathrm{SNR}}\right)^2\right]\Big/\left(N_a N_e\right)\right\}} \quad (1)$$

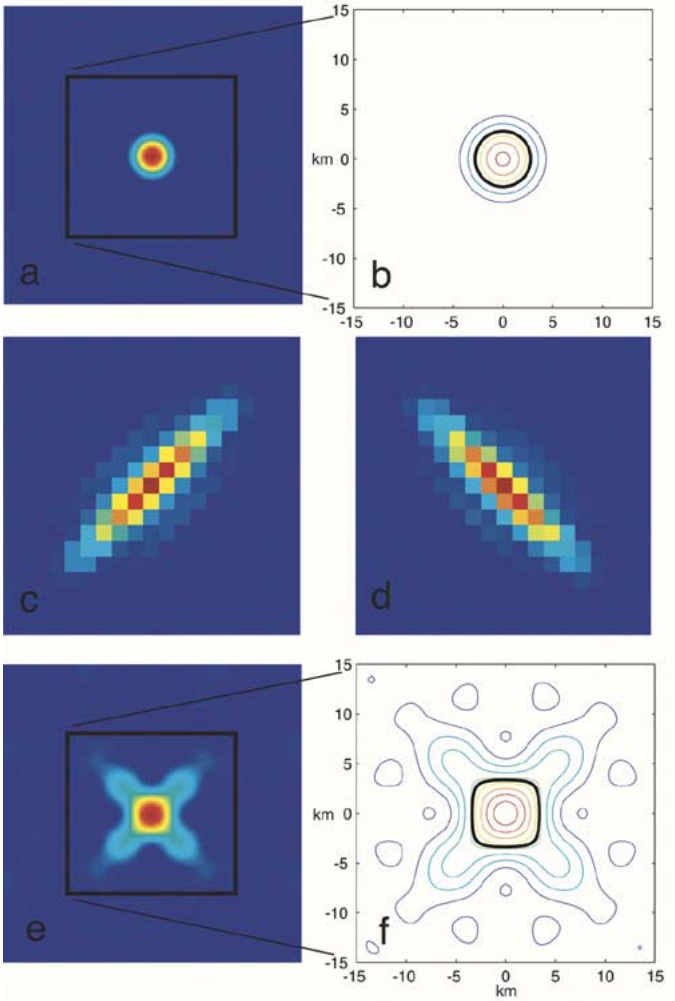

Fig. 9. Two-dimensional simulation azimuth angle of 45° using 3-km azimuth averaged measurements. The simulation images cover an area approximately 50 × 50 km in size and show the estimated normalized radar backscatter in linear space. The contour plots are expanded views 30 × 30 km in size. (Top row) The synthetic "true" signal (a) image and (b) contour plot. (Second row) Averaged measurements are shown in the second row for (c) forward-looking and (d) aft-facing measurements. (Bottom row) SIR algorithm reconstruction result (e) image, and (f) contour plot. Color scales and contour levels arbitrary, except the thick black contour which corresponds to the 3-dB contour.

where N_e is the number of independent range looks determined by the range compression, and N_a is the effective number of independent azimuth looks in each averaged measurement. Combining the number of range and azimuth looks yields a variation of from 12–80 looks per cell over the swath. Over land, the HYDROS SNR is generally high so that the measurement K_p is primarily determined by the number of looks [20].

Two Monte Carlo simulation approaches are employed. In the first, the reconstruction performance is evaluated in detail at discrete swath locations. In the second, full-swath reconstruction is simulated. Discrete swath location simulation is considered first.

In the discrete swath location simulation, 3-km azimuth averaging is used to generate simulated low-resolution radar measurements. These have nominal 3-dB resolutions of approximately 3 km × 30 km. The HYDROS antenna/orbit geometry determines the sampling locations. In the simulation, the synthetic "true" surface radar backscatter cross section (sigma-0)

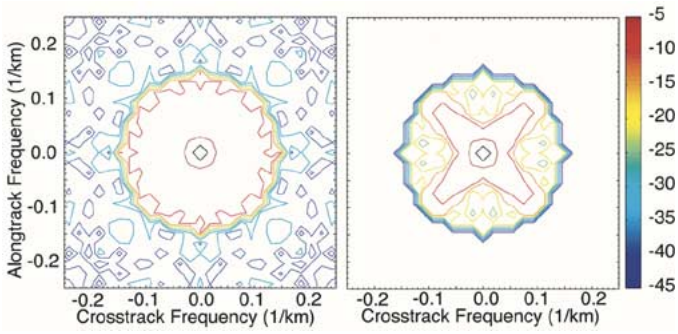

Fig. 10. Spectra of 3-km reconstruction at an azimuth angle of 45°. Axes are in 1/km. Scales are in decibels. (Left) True signal spectrum. (Right) SIR signal estimate spectrum. The 3-dB width of both spectra are similar, though the sidelobe structures differ somewhat.

is a single low-pass filtered delta function to enable visualization of the point-response function. The low-pass filter ensure that the true surface is bandlimited to 3-km resolution. Monte Carlo noise is added to the simulated based on the estimated SNR and number of looks [(1); see [24]].

A sample discrete swath simulation result at an antenna azimuth angle of 45° (within the swath "sweet spot") is shown in Fig. 9. The "raw" image shows the individual 3-km measurements for each look direction. The relative density and spacing of the individual LBR measurements are evident by the image gridding. These are the nonenhanced images. The SIR image better represents the original signal, though for this case the original signal is incompletely recovered and contains low-level "star-like" artifacts due to the elongated response functions. The 3-dB resolution is approximately 6 km in the vertical and horizontal directions, but only 9 km in the diagonal directions. We note that similar enhancement performance can be achieved even if the measurements are averaged to 9 km in azimuth by 6 km in range resolution. The corresponding spectra of the signals in Fig. 9 are shown in Fig. 10. The reconstructed signal spectrum approaches the original signal spectrum at some directional orientations; however, at other directions, the signal spectrum is less completely recovered, confirming that the reconstructed signal has better effective resolution at some directions than others. At this swath location, the finest (best case) resolution is aligned along 45° or 135°, while the resolution at 0° and 90° is slightly coarser.

To aid in tradeoff studies, we evaluate the best and worst case resolutions by examining the spectrum of the recovered signal and reporting the smallest and largest 3-dB spectral widths. The precise values for the recovered resolution are dependent on the orientation of the slices, which varies with swath location.

Fig. 11 plots the resolution performance metrics for the 3-km simulations. In this simulation example, the reconstruction is able to recover the signal at 6-km resolution over most of the swath, based on the best case orientation. However, the worst case resolution varies from approximately 22 km at far swath and nadir where the fore and aft slices are aligned to ∼8 km at midswath where the slice orientation is the most favorable (the elongated slices are orthogonal). A useful measure for the effective resolution is the square root of the area for which the response is 3-dB or less down from the peak. Using this

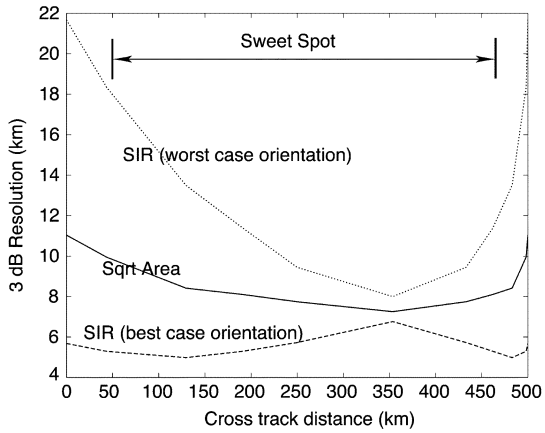

Fig. 11. Resolution metric (3-dB peak width) versus crosstrack distance from nadir for the 3-km resolution averaged measurements. Resolution varies with angle. (Dashed line) Best case SIR. (Dotted line) Worst case angle. (Solid line) Square-root area metric.

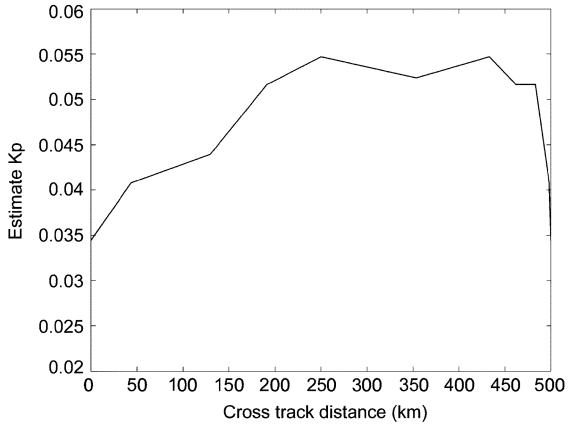

Fig. 12. Average (over a local area) of the normalized standard deviation (K_p) of the reconstructed backscatter versus swath location.

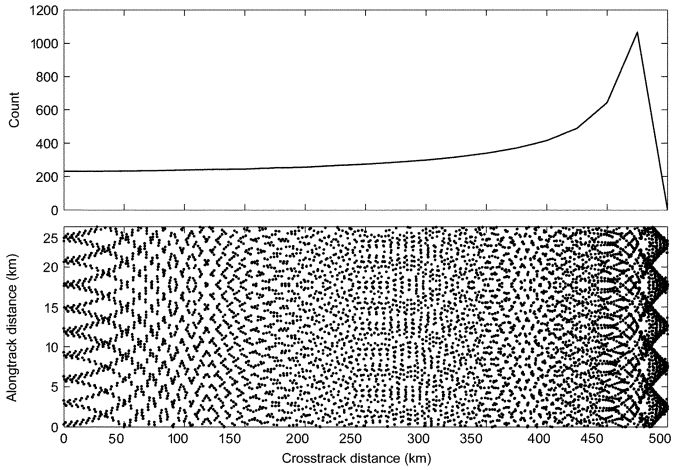

Fig. 13. (Bottom) Locations of individual low-resolution measurements from both forward-looking and aft-looking measurements over the right-side swath. (Top) Count of the number of low-resolution measurements in a 25 km × 25 km area as a function crosstrack position. The variations in density and position are the result of the scanning geometry and PRF.

metric, over the swath "sweet spot," the effective resolution by the square-root area metric is better than 10 km. We note that at nadir and far swath, the reconstruction is, in effect, azimuth-only, since the fore and aft slices are aligned. At midswath, however, reconstruction from fore/aft measurements significantly improves the recoverable resolution.

As previously noted, reconstruction to improve the spatial resolution tends to degrade the SNR. To quantify the noise, we plot the K_p of the backscatter estimates as a function of swath location in Fig. 12. Since spatial resolution improves with increasing SIR iterations but SNR degrades, there is a tradeoff between SNR and spatial resolution.

Careful analysis reveals that the correlation between pulses due to coherence of Rayleigh fading increases the K_p of the averaged measurements only marginally [24]. While reconstruction increases the noise, the combining of forward-looking and aft-looking measurements provides additional averaging, thereby reducing the noise. The result is that the K_p of the reconstructed low-resolution measurements is similar to the K_p of the raw measurements for a single direction. We note that K_p varies over the swath in inverse proportion to the number of effective looks, which is related to the effective resolution of the reconstruction. As the resolution of the reconstruction improves, K_p increases. We note that the K_p value of $\sim$0.05 achieved over the "sweet spot" is approximately the same obtained by degrading the baseline 3-km SAR measurements ($Kp = 0.15$) from 3–9 km (a factor of $\sqrt{9} = 3$ reduction in noise).

We further note that the reconstruction is essentially an incoherent process. The SAR-type processing planned in the baseline HYDROS non-real-time processing is, however, coherent and can produce significantly better resolution (1 versus 8 km) over the "sweet spot" portion of the swath. However, due to the relative variation of iso-range and iso-Doppler lines over the swath, the resolution of SAR processing varies over the swath (see Fig. 2). At nadir and far-swath, the reconstruction, which accounts for the roll off of the antenna pattern, yields slightly finer resolution (22 km) than the baseline SAR processing (28 km).

V. Full-Swath Simulation

Finally, a simple 2-D simulation over a full half swath (results are symmetric for both sides of the swath) is generated to better understand the varying reconstruction performance over the swath due to the varying orientation of the slices. In order to ensure a conservative performance assessment, for this simulation the azimuth averaging was set at 8 km, while the range averaging was set at 5 km. The center locations of each of the range-compressed azimuth-filtered slice measurements are shown in Fig. 13 as computed from the nominal orbit, PRF, and antenna geometry. We note the dense sampling of the surface afforded by the slice measurements. This dense sampling is essential for successful reconstruction [5].

Simulation results for this case are shown in Fig. 14. A synthetic true "scene," consisting of several point targets and lines and bandlimited to 5 km, is used to generate simulated slice measurements based on the predicted antenna pattern and sampling geometry. Note that in this simulation, the slice orientations vary across the swath resulting in variable reconstruction

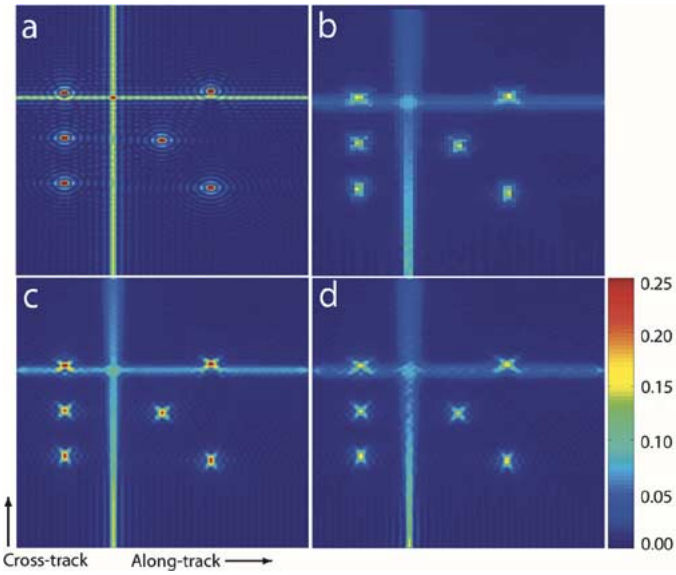

Fig. 14. Two-dimensional noise-free swath simulation results with a 5-km resolution "true" signal and 5-km sampling. Only the left-half swath is shown with the nadir track extending from left to right along the bottom edge of the 500 km × 500 km image. (a) Synthetic true image. (b) Gridded nonenhanced raw measurements. (c) Noise-free SIR image estimate. (d) Noisy SIR image estimate. Note variation in along-track resolution with crosstrack position as evidenced by the vertical (crosstrack) line. This is due to the varying geometry of the fore/aft measurement overlap.

performance. Image estimates resulting from gridding the measurements (no reconstruction) and the SIR reconstruction algorithms are shown in Fig. 14. As anticipated, the SIR algorithm provides the finest resolution and best signal reconstruction, but contains image artifacts. The variable reconstruction with azimuth angle is evident in the vertical line and in the variations in the star-like artifacts surrounding the point targets. For the noisy results shown in Fig. 14, Monte Carlo noise based on the calculated SNR is added. The resulting SIR images are somewhat degraded and have reduced dynamic range, but do a reasonable job of reconstructing the surface backscatter, except at far (and near) swath where the azimuth geometry is unfavorable. These results demonstrate the viability of the approach, though further tuning to optimize its performance for HYDROS is suggested. Though performance is not as good as the baseline SAR-type processing, the reduced computational and data requirements of the fore/after reconstruction approach will enable real-time product generation.

VI. Conclusion

The HYDROS mission will provide a capability for high spatial resolution sampling of soil moisture. The SAR-like range/Doppler processing required to achieve the finest resolution may be unsuitable for some real-time downlink and operational purposes. In this paper, we have considered an alternate downlink and processing approach based on onboard preaveraging of the measurements and application of reconstruction techniques in ground processing. This lowers the downlink data rate and simplifies initial processing steps.

Two approaches to reconstruction were considered: azimuth-only and combined fore/aft-looking. While reconstruction increases the noise, the low-resolution measurements and the combining of forward-looking and aft-looking measurements provides averaging, thereby reducing the noise. The result is that the K_p of the reconstructed low-resolution measurements is similar to the K_p of the raw measurements for the forward-looking direction. We note that K_p varies over the swath in inverse proportion to the number of effective looks, which is related to the effective resolution of the reconstruction. As the resolution of the reconstruction improves, K_p degrades.

Of the two approaches explored for HYDROS reconstruction and resolution enhancement, using fore- and aft-looking measurements is shown capable of achieving better than the desired 10-km spatial resolution from low-data-rate HYDROS measurements with acceptable signal fidelity and noise level over most of the swath.

These results suggest that the approach is, thus, a viable low-cost option for real-time processing of data for the HYDROS mission. Additional studies are planned to optimize the selection of azimuth and range averaging, to evaluate the sensitivity of the reconstruction to the full 2-D antenna pattern, the PRF, and the averaging filter response functions, and to refine the ground processing algorithms.

References

[1] E. Attema, "The active microwave instrument onboard the ERS-1 satellite," *Proc. IEEE*, vol. 79, no. 6, pp. 791–799, Jun. 1991.

[2] F. Naderi, M. H. Freilich, and D. G. Long, "Spaceborne radar measurement of wind velocity over the ocean—An overview of the NSCAT scatterometer system," *Proc. IEEE*, vol. 79, no. 6, pp. 850–866, Jun. 1991.

[3] M. W. Spencer, C. Wu, and D. G. Long, "Improved resolution backscatter measurements with the seawinds pencil-beam scatterometer," *IEEE Trans. Geosci. Remote Sens.*, vol. 38, no. 1, pp. 89–104, Jan. 2000.

[4] F. T. Ulaby, R. K. Moore, and A. K. Fung, *Microwave Remote Sensing—Active and Passive*. Reading, MA: Addison-Wesley, 1981.

[5] D. S. Early and D. G. Long, "Image reconstruction and enhanced resolution imaging from irregular samples," *IEEE Trans. Geosci. Remote Sens.*, vol. 39, no. 2, pp. 291–302, Feb. 2001.

[6] R. R. Forster, D. G. Long, K. C. Jezek, S. D. Drobot, and M. R. Anderson, "The onset of arctic sea-ice snowmelt as detected with passive- and active-microwave remote sensing," *Ann. Glaciol.*, vol. 33, pp. 85–93, 2001.

[7] P. Lecomte, A. Cavanie, and F. Gohin, "Recognition of sea ice zones using ERS-1 scatterometer data," in *Proc. IGARSS*, 1993, pp. 855–857.

[8] D. G. Long, M. R. Drinkwater, B. Holt, S. Saatchi, and C. Bertoia, "Global ice and land climate studies using scatterometer image data," *EOS, Trans. Amer. Geophys. Union*, vol. 82, no. 43, p. 503, Oct. 23, 2001.

[9] D. G. Long and M. R. Drinkwater, "Cryosphere applications of NSCAT data," *IEEE Trans. Geosci. Remote Sens.*, vol. 37, no. 3, pp. 1671–1684, May 1999.

[10] V. R. Wismann, K. Boehnke, and C. Schmullius, "Monitoring ecological dynamics in Africa with the ERS-1 scatterometer," in *Proc. IGARSS*, 1995, pp. 1523–1525.

[11] M. J. McFarland, R. L. Miller, and C. M. U. Neale, "Land surface temperature derived from the SSM/I passive microwave brightness temperatures," *IEEE Trans. Geosci. Remote Sens.*, vol. 28, pp. 839–845, Sep. 1990.

[12] T. J. Jackson and T. J. Schmugge, "Algorithm for the passive microwave remote sensing of soil moisture," in *Microwave Radiometry and Remote Sensing Applications*, P. Pampaloni, Ed. Zeist, The Netherlands: VSP, 1989, pp. 3–17.

[13] E. G. Njoku and D. Entekhabi, "Passive microwave remote sensing of soil moisture," *J. Hydrol.*, vol. 184, pp. 101–129, 1996.

[14] E. Njoku, W. Wilson, S. Yueh, and Y. Rahmat-Samii, "A large-antenna microwave radiometer-scatterometer concept for ocean salinity and soil moisture sensing," *IEEE Trans. Geosci. Remote Sens.*, no. 6, pp. 2645–2655, Nov. 2000.

[15] P. Pampaloni and S. Paloscia, "Microwave emission and plant water content: A comparison between field measurement and theory," *IEEE Trans. Geosci. Remote Sens.*, vol. GE-24, pp. 900–904, 1986.
[16] D. Cline, Ed., "Cold Land Processes Mission (EX-7), Report of the NASA Post-2002 Land Surface Hydrology Planning Workshop, NASA Land Surface Hydrology Program (LHSP)," NASA, Irvine, CA, [Online]. Available: http://lshp.gsfc.nasa.gov, Apr. 12–14, 1999.
[17] T. Jackson, Ed., "Soil Moisture Mission (EX-4), Report of the NASA Post-2002 Land Surface Hydrology Planning Workshop, NASA Land Surface Hydrology Program (LHSP)," NASA, Irvine, CA, [Online]. Available: http://lshp.gsfc.nasa.gov, Apr. 12–14, 1999.
[18] E. Njoku, M. Spencer, K. McDonald, J. Smith, P. Houser, T. Doiron, P. O. Neill, R. Girard, and D. Entekhabi, "The HYDROS mission: Requirements and system design," in *Proc. IEEE Aerospace Conf.*, Big Sky, MT, Mar. 7–12, 2004.
[19] D. Entekhabi *et al.*, "The Hydrosphere State (HYDROS) mission concept: An earth system pathfinder for global mapping of soil moisture and land freeze/thaw," *IEEE Trans. Geosci. Remote Sens.*, vol. 43, no. 10, pp. 2184–2195, Oct. 2004.
[20] M. W. Spencer, W.-Y. Tsai, and D. G. Long, "High resolution measurements with a spaceborne pencil-beam scatterometer using combined range/doppler discrimination techniques," *IEEE Trans. Geosci. Remote Sens.*, vol. 41, no. 3, pp. 567–581, Mar. 2003.
[21] D. G. Long and D. L. Daum, "Spatial resolution enhancement of SSM/I data," *IEEE Trans. Geosci. Remote Sens.*, vol. 35, no. 2, pp. 407–417, Mar. 1998.
[22] D. G. Long, P. Hardin, and P. Whiting, "Resolution enhancement of spaceborne scatterometer data," *IEEE Trans. Geosci. Remote Sens.*, vol. 31, pp. 700–715, May 1993.
[23] P. K. Yoho and D. G. Long, "An improved scatterometer simulation model for spaceborne scatterometer measurements," *IEEE Trans. Geosci. Remote Sens.*, vol. 41, no. 11, pp. 2292–2685, Nov. 2003.
[24] ——, "Correlation and covariance of satellite scatterometer measurements," *IEEE Trans. Geosci. Remote Sens.*, vol. 42, no. 6, pp. 1176–1187, Jun. 2004.

David G. Long (S'80–SM'98) received the Ph.D. degree in electrical engineering from the University of Southern California, Los Angeles, in 1989.

From 1983 to 1990, he was with the National Aeronautics and Space Administration (NASA) Jet Propulsion Laboratory (JPL), Pasadena, CA, where he developed advanced radar remote sensing systems. While at JPL, he was the Senior Project Engineer on the NASA Scatterometer (NSCAT) project, which was flown aboard the Japanese Advanced Earth Observing System (ADEOS) from 1996 to 1997. He was also the Experiment Manager and Project Engineer for the SCANSCAT scatterometer (now known as SeaWinds). In 1990, he joined the Department of Electrical and Computer Engineering, Brigham Young University (BYU), Provo, UT, where he currently teaches upper division and graduate courses in communications, microwave remote sensing, radar, and signal processing, is the Director of BYU's Center for Remote Sensing, and is the Head of the Microwave Earth Remote Sensing Laboratory. He is the Principal Investigator on several NASA-sponsored interdisciplinary research projects in microwave remote sensing and innovative radar systems. He has numerous publications in signal processing and radar scatterometry. His research interests include microwave remote sensing, radar, polar ice, signal processing, estimation theory, and mesoscale atmospheric dynamics. He has over 250 publications in the open literature.

Dr. Long has received the NASA Certificate of Recognition several times. He is an Associate Editor for the IEEE GEOSCIENCE AND REMOTE SENSING LETTERS.

Michael W. Spencer received the B.S. degree in physics from The College of William and Mary in Virginia, Williamsburg, in 1985, the M.S. degree in planetary science from the California Institute of Technology (Caltech), Pasadena, in 1987, the M.S. degree in electrical engineering from the University of Southern California, Los Angeles, in 1995, and the Ph.D. degree in electrical engineering from Brigham Young University, Provo, UT, in 2001.

From 1987 to 1990, he was with the Aerospace Corporation, Los Angeles, CA, where he was involved in the modeling and analysis of advanced meteorological and surveillance systems. He has been with the Jet Propulsion Laboratory, Caltech, since 1990, where he has worked on the conceptualization, system design, simulation, and calibration of radar remote sensing instruments. He is currently managing the development of the HYDROS instrument.

Eni G. Njoku (M'77–SM'83–F'95) received the B.A. degree in natural and electrical sciences from Cambridge University, Cambridge, U.K., in 1972, and the M.S. and Ph.D. degrees in electrical engineering from the Massachusetts Institute of Technology, Cambridge, in 1974 and 1976.

He is currently a Principal Scientist with the Jet Propulsion Laboratory (JPL), Pasadena, CA, and is the JPL Project Scientist for the HYDROS mission. From 1976 to 1977, he was a National Research Council Resident Research Associate. In 1977, he joined JPL. From 1986 to 1990, he served as Discipline Scientist for Ocean and Earth Science Data Systems at NASA Headquarters, Washington, DC, and from 1993 to 1994, he was Manager of the Geology and Planetology Section at JPL. During the 2001–2002 academic year, he was on leave as a Visiting Professor at the Massachusetts Institute of Technology. He is a member of the Aqua Advanced Microwave Scanning Radiometer science team and was Principal Investigator for the IIP OSIRIS technology study. His primary interests are in the use of passive and active microwave remote sensing for hydrology and climate applications. His research involves studies of microwave interactions with land surfaces and retrieval algorithm development.

Dr. Njoku is a member of the American Meteorological Society, the American Geophysical Union, the American Association for the Advancement of Science, Commission F of the International Union of Radio Science, and Sigma Xi. He has served as an Associate Editor of the IEEE TRANSACTIONS ON GEOSCIENCE AND REMOTE SENSING (1985–1988) and was the Technical Program Chairman for IGARSS'94 held in Pasadena, CA. He has been a recipient of NASA Group Achievement Awards in 1980, 1982, and 1985, and he was awarded the NASA Exceptional Service Medal in 1985.